Shifts in phenology and species ranges restructure the flowering season across North America

Authors: Tadeo H. Ramirez-Parada[1], Isaac W. Park[2], Shijia Peng[3], Misako Nishino[4], John T. Kartesz[4], Sydne Record[5], Charles C. Davis[6], Susan J. Mazer[1].

Institutional Affiliations: [1]Department of Ecology, Evolution, and Marine Biology, University of California, Santa Barbara, CA 93106, USA. [2]Department of Biology, Georgia Southern University, Statesboro, GA 30460, USA. [3]Department of Earth Sciences, University of Oxford, Oxford OX1 3AN, UK. [4]Biota of North America Program (BONAP), Chapel Hill, 27516, North Carolina, USA [5]Department of Wildlife, Fisheries, and Conservation Biology, University of Maine, Orono, ME, 04469, USA. [6]Department of Organismic and Evolutionary Biology, Harvard University, Cambridge, MA 02138, USA.

Contact: Tadeo H. Ramirez-Parada, tadeoramirezp@gmail.com

Abstract

Global change is altering the phenology and geographic ranges of flowering species, with potentially profound consequences for the timing and composition of floral resources and the seasonal structure of ecological communities. However, shifts in flowering phenology and species distributions have historically been studied in isolation due to disciplinary silos and limited data, leaving critical gaps in our understanding of their combined effects. To address this, we used millions of herbarium and occurrence records to model phenological and range shifts for 2,837 plant species in the United States across historical, recent, and projected climate and land cover conditions, enabling us to scale responses from species to communities, and from local to continental geographies. Our analysis reveals that communities are shifting toward earlier, longer flowering seasons in most biomes, with co-flowering species richness increasing at the edges of the season and declining at historical peaks—trends projected to intensify under ongoing environmental trends. Although these shifts operate concurrently, they affect different aspects of the flowering season: phenological changes primarily alter seasonality—its start, end, and duration—and co-flowering diversity at the edges of the season, while range shifts more strongly influence co-flowering species richness during historical seasonal peaks, and attributes tied to community composition, such as patterns of flowering synchrony among co-occurring species. Together, these results demonstrate that shifts in phenology and species ranges act synergistically to restructure the flowering seasons across North America, revealing wide variation in the pace and magnitude of change among biomes.

Introduction

The timing, duration, and species composition of a community's flowering season influences both plant fitness and the survival and reproduction of organisms that depend on floral resources. These attributes can mediate pollinator population growth rates (1) and various density-dependent ecological outcomes in plants—such as pollination or florivory—that can impact population persistence and the evolution of life-history strategies (2). Recent climate and land use changes have led to widespread shifts in flowering phenology and plant distributions (3, 4), often disrupting ecological interactions through altered spatial and seasonal synchrony between species (5, 6). However, how species-level shifts in phenology and distributions scale to jointly affect community-level flowering patterns is poorly understood, largely because these processes have historically been studied separately (7), but also because long-term datasets including enough species to characterize a community's flowering season are rare and often temporally and spatially limited (8). Elucidating how shifts in phenology and species ranges affect the structure of the flowering season from species to communities—and understanding how these effects are distributed across regions and biomes—is essential for forecasting the impacts of global change on terrestrial ecosystems.

To address this knowledge gap, we assembled a dataset of over 2.7 million herbarium and community-science records from 2,837 species to examine how climate change affects the structure of the flowering season in the conterminous United States (CONUS). We modeled each species' geographic distribution under historical, current, and future climate conditions, also accounting for land cover and land use changes. Additionally, we assessed how interannual variation in temperature and precipitation—independently and interactively—influence the onset, termination, and duration of the flowering period for each species. By concurrently predicting species occurrences and their flowering periods across sites, these analyses allowed us to evaluate the effects of environmental change on flowering patterns at scales ranging from individual species to communities and from local to continental extents. Specifically, throughout CONUS, we measured how recent and future environmental change affects i) the start of the flowering season (SOS), ii) the end of the flowering season (EOS), iii) the duration of the flowering season (DOS), iv) the richness of co-flowering species each day of the year, and v) the network of pairwise flowering synchronies between co-occurring species, which determines the potential for flowering-mediated interactions between species.

Our analyses enabled us to test several hypotheses about the relative impacts of shifts in phenology and species ranges on the structure of the flowering season (Fig. 1). Phenological responses to climate tend to differ markedly among species flowering early and late in the season. For example, spring-flowering species tend to advance flowering in response to warming versus late summer- and fall-flowering species, which typically show limited responsiveness or flowering delays (9, 10). In contrast, changes in species diversity typically impact species-level phenology indirectly (e.g., through changes in soil nitrogen or moisture) (11), and species lost or gained within most communities do not tend to flower predominantly early or late within the season (but see counterexamples among invasive species) (12, 13). Because phenological responses generate consistent shifts among species at both ends of the flowering season, changes in attributes of the season related to timing—such as its start, end, and duration—should be more strongly mediated by phenological responses than by range shifts (Fig. 1B-D) (14). Conversely, the richness of flowering concurrently during a community's flowering peak—during which relatively few taxa are initiating or terminating flowering (Fig. 1B-D)—or attributes of the season tied to community composition (e.g., the network of flowering synchronies between co-occurring species) (Fig. 1E, F) should be more strongly influenced by species gains and losses due to range shifts than by plastic responses of flowering phenology. This is because phenological shifts redistribute existing flowering diversity and change the degree of flowering synchrony between species (i.e., nodes in the flowering network), whereas range shifts add or remove species from the community. Therefore, phenological shifts change the strength of the connections between nodes in the flowering network (Fig. 1E), whereas range shifts add nodes or subtract them altogether, thereby creating or removing many connections at once (Fig. 1F).

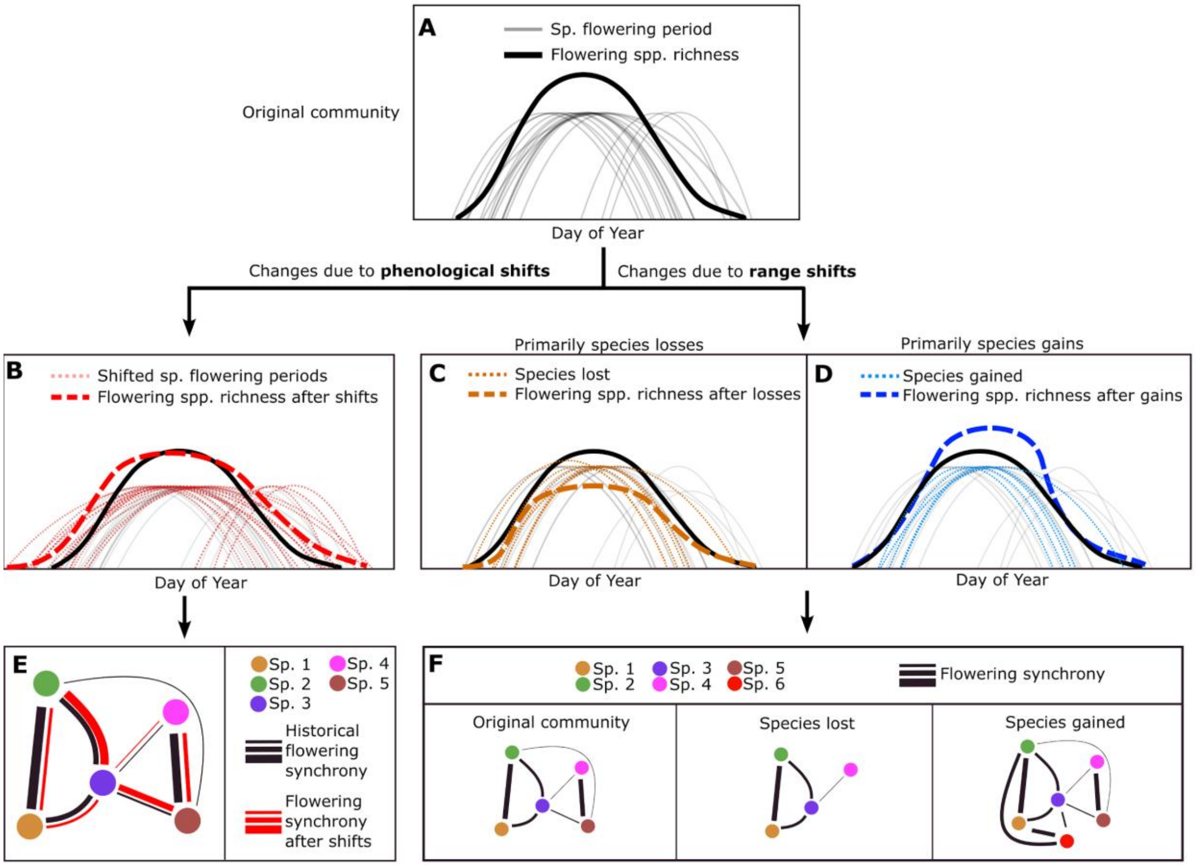

Figure 1—Hypothetical effects of shifts in phenology and species ranges on the structure of the flowering season. **A** shows historical phenological patterns in a community, with grey lines showing the flowering periods of individual species, and the solid black line depicting the historical species richness of co-flowering species throughout the year. **B** shows changes in community-level flowering caused by shifts in phenology among species alone, and depicts a scenario in which early-flowering species tend to advance and late-flowering species to delay their flowering, and in which species primarily extend their flowering relative to historical These changes are predicted to conditions. primarily impact the start, end, and duration of the season, as well as the richness of flowering species early and late in the season. **C** and **D** show shifts in community-level flowering patterns caused by shifts in species ranges alone, respectively showing scenarios in which range shifts generate species losses or species gains in the focal community, and assuming gained or lost species do not tend to flower during a specific season. Such changes should primarily impact the richness of the flowering season during the peak of the season, during which most species gained or lost are likely to have already started flowering. **E** shows the effects of phenological shifts on patterns of pairwise flowering synchronies for a simple network of 5 species, and **F** depicts the effects of species losses or gains due to range shifts on the same network, with line widths indicating the degree of flowering synchrony between two species. Line colors in **E** depict flowering synchronies before and after shifts in flowering phenology due to environmental change. Shifts in phenology should alter the degree of overlap between species, with the weakest links most at risk of being lost under environmental change. In turn, species losses or gains should have more profound effects by creating or removing flowering synchronies among many species at once.

Phenology and species distributions are primarily mediated by different environmental factors, so different environmental variables should also have distinct impacts on the structure of the season. For example, temperature—through winter chilling, spring forcing, or autumn cooling—is typically the predominant driver of phenology among species in the temperate zone (15), with precipitation having a more pronounced role in arid and semi-arid regions than in mesic ones (16, 17). In turn, shifts in plant species composition have been primarily linked to variation in precipitation (18–20). Therefore, through their respective effects on phenological responses and species turnover, we would predict that changes in temperature will more strongly mediate shifts in the start, end, and duration of the season, with precipitation more strongly mediating shifts in co-flowering species richness during the peak of the season and patterns of pairwise flowering synchrony among co-occurring species instead. In turn, land use change—such as urbanization or agricultural intensification—should more strongly impact species composition than phenology through direct removal or replacement of vegetation cover, resulting in associations between changes in land and in co-flowering species richness during the historical seasonal period of peak flowering. We similarly expect land use changes to influence the network of flowering synchronies among species.

Together, these analyses offer the most comprehensive assessment of how recent and projected global change impacts flowering patterns in North American floras, revealing wide heterogeneity in the severity of flowering reassembly across biomes.

Results

Changes to the start, duration, and end of the flowering season

Shifts in species ranges and flowering phenology altered the flowering season's start (SOS), end (EOS), and duration (DOS) across all ecoregions. SOS predominantly advanced between the historical and recent periods (Fig. 2A). EOS was delayed in Eastern ecoregions, while responses in the West were more variable (e.g., some areas of the Western Cordillera exhibited delays, others did not) (Fig. 2A). SOS and EOS generally moved in opposite directions, with SOS showing larger shifts towards earlier dates where SOS and EOS moved in the same direction; consequently, the flowering season duration (DOS) increased across most of CONUS (Fig. 2A). Future environmental conditions were projected to generate more drastic changes, with greater

SOS advances and fewer areas showing SOS delays (e.g., Warm Deserts) (Fig. 2B). EOS delays were projected to be greater and more consistent across regions than in recent decades (Fig. 2B). As a result, DOS was predicted to increase further across most of CONUS (Fig. 2B).

Across ecoregions, shifts in the timing of the season between the historical and recent periods were primarily caused by shifts in flowering phenology (Fig. 2C). However, in each ecoregion, seasonal changes within a substantial proportion of sites were caused primarily by shifts in species ranges, which predominated overall as drivers of EOS shifts in some ecoregions (e.g., Upper Gila Mountains, and prairies within the great plains) (Fig. 2C). Phenological shifts were also projected to be the primary drivers of changes in SOS, EOS, and DOS between recent and future climatic conditions in most ecoregions (Fig. 2C). However, range shifts were projected to predominate over phenological responses in some ecoregions (e.g., Western Sierra Madre Piedmont, Atlantic Highlands), while the predominance of phenology over range shifts was projected to accentuate in others (e.g., Temperate Prairies, Mixed Wood Shield) (Fig. 2C).

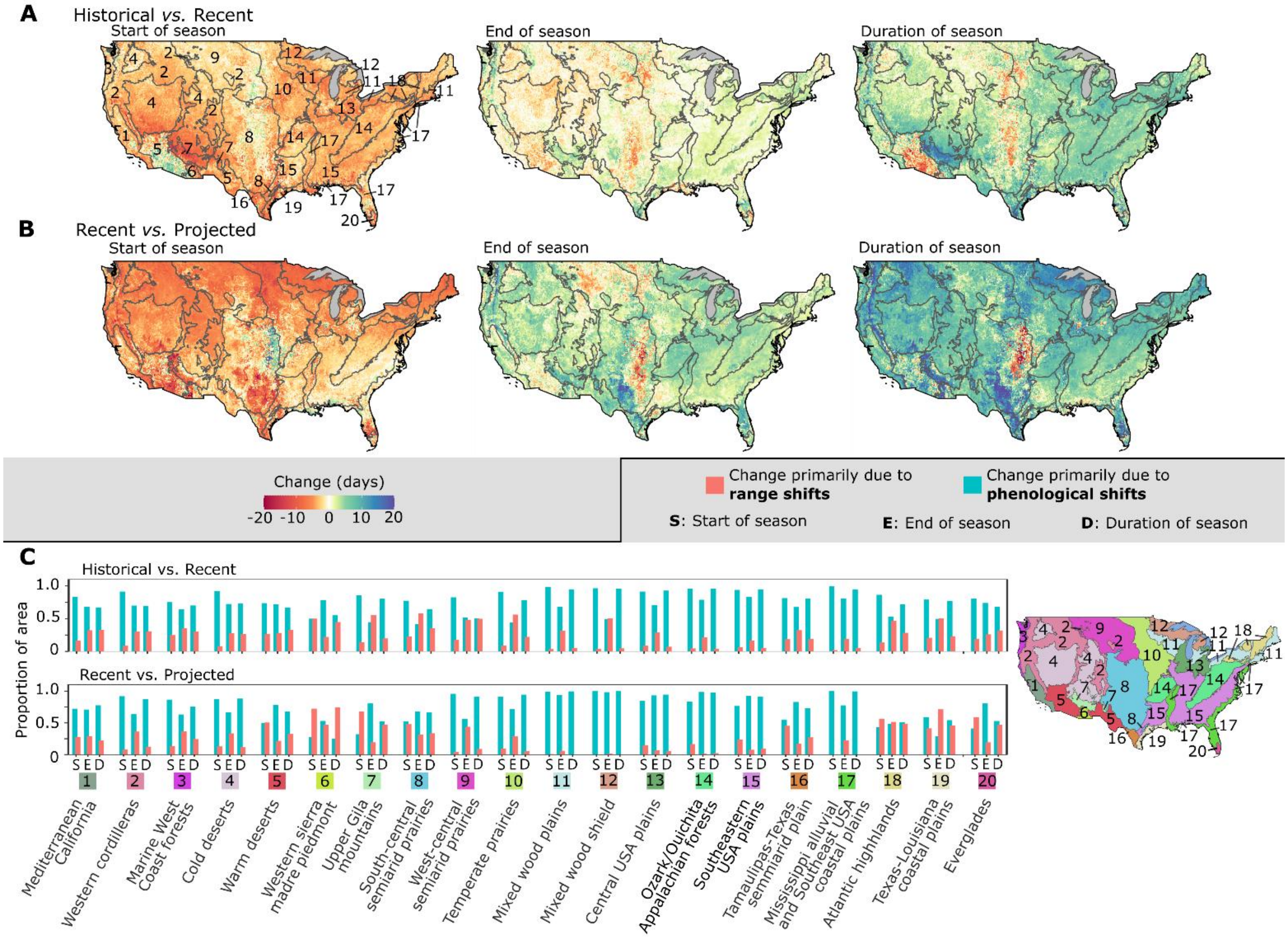

Figure 2—Changes in the start, end, and duration of the flowering season under recent and projected climatic and land cover change, and the relative contributions of shifts in phenology vs. species ranges to these changes. **A** depicts changes in the start, end, and duration of the season predicted between the historical (1961-1980) and recent (2001-2020) periods. **B** shows predicted changes between recent conditions and future conditions expected under 2°C of warming and land cover patterns for the year 2080 under the Special Report on Emissions Scenario (SRES) B1. **C** shows the proportion of area within each level II ecoregion throughout CONUS (map subdivisions labeled 1-20, also shown in A) for which shifts in phenology or in species ranges were the primary contributors to observed change. For graphing, the color scale in **A** and **B** was capped to the central 99% of the data to avoid distortion of the range from extreme values. Grid cells in **A** and **B** have a resolution of 12×12 km.

Changes in the seasonal distribution of co-flowering species richness

Co-flowering species richness remained mostly unchanged during the winter months preceding the flowering season in most regions, but increased by February in low-latitude ecoregions where spring starts early (e.g., Warm Deserts) (Fig. 3A). Significant changes were widespread in

March, April, and May, which predominantly showed increases due to the earlier onset of spring across CONUS. Decreases first occurred in April and May in regions experiencing early onset of summer drought (e.g., Warm Deserts, South-Central Semi-Arid Prairies). More ecoregions experienced declines in co-flowering richness during summer, with the onset of declines occurring earlier in the year in arid ecoregions (e.g., May to June for Cold Deserts vs. June to July for the Western Cordillera). Fall changes were smaller across CONUS, except in some regions within the Great Plains (e.g., South-Central Semi-arid Prairies).

In most ecoregions, changes in co-flowering species richness early in the season were primarily generated by phenological shifts, with range shifts exerting a greater influence later in the season and predominating during late spring and summer (May-Sep; Fig. 3B). The predominant drivers of changes in co-flowering species richness near the end of the season varied among ecoregions, with shifts in phenology predominating in some (e.g., Warm Deserts) and range shifts in others (e.g., Temperate prairies). In turn, change in some ecoregions were predominantly caused by either shifts in phenology or species ranges year-round (e.g., South-Central Semi-arid Prairies and Western Cordilleras).

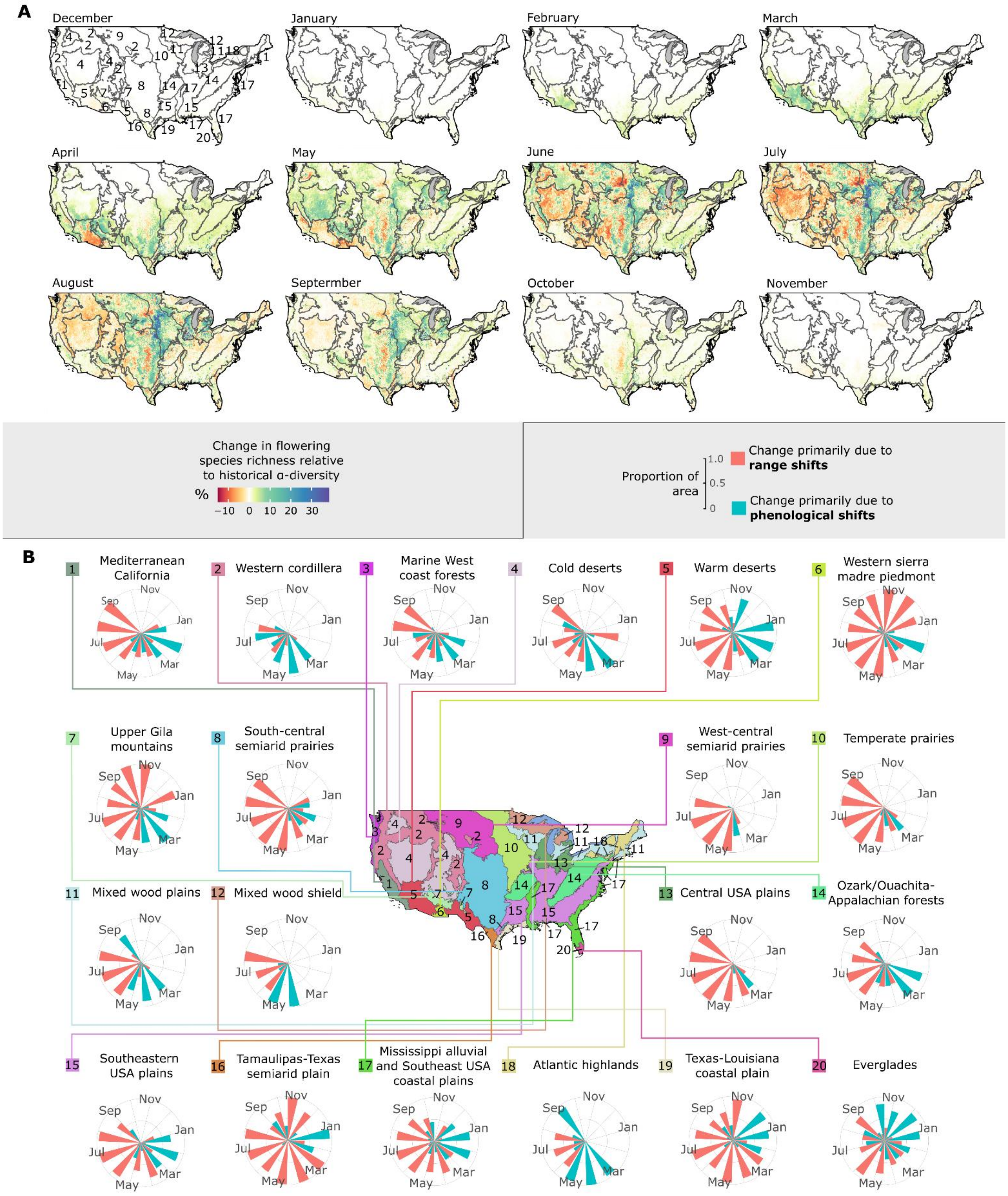

Figure 3—Changes between historical period (1961-1980) and the recent period (2001-2020) in the richness of co-occurring species flowering each month across the conterminous United States. **A** shows

the change co-flowering richness each month for each location relative to the total species diversity of that site during the historical period (1961-1990). **B** shows the proportion of sites within each ecoregion (map subdivisions labeled 1-20) for which range shifts or phenological shifts were the primary cause of observed changes in the diversity of flowering species that month. For graphing, the color scale in **A** was capped to the central 99% of values to avoid distortion from extreme values. Grid cells in **A** have a resolution of 12×12 km.

Under projected climate conditions, decreases in co-flowering species richness were larger and more widespread across ecoregions than the decreases observed in recent decades (Fig. 4). Compared to recent decades, increases co-flowering richness during spring were weaker, and declines occurred earlier and were more severe in many ecoregions (e.g., Warm Deserts, Mediterranean California) (Fig. 4A). Summer and fall decreases in co-flowering richness were most severe across ecoregions in the Great Plains, but were also widespread across the West. In contrast, co-flowering species richness was projected to moderately increase during summer and fall in many Eastern ecoregions (e.g., Southeast USA Plains, Southeast USA Coastal Plain).

Under projected environmental changes, and for most ecoregions, phenological shifts were the primary causes of changes in co-flowering species richness early and late in the season (Fig. 4B). Phenological shifts predominated throughout the year in some ecoregions (e.g., Mixed Wood Shield, Atlantic Highlands). However, the relative influence of range shifts increased throughout the year, becoming the predominant cause of year-round changes in co-flowering richness in more ecoregions than observed between the historical and recent periods (e.g., Temperate Prairies, Texas-Louisiana Coastal Plain). Indeed, range shifts were the overwhelming cause of changes in co-flowering richness during summer and fall in regions showing the most severe decreases (e.g., South Central Semi-Arid Prairies, Temperate Prairies).

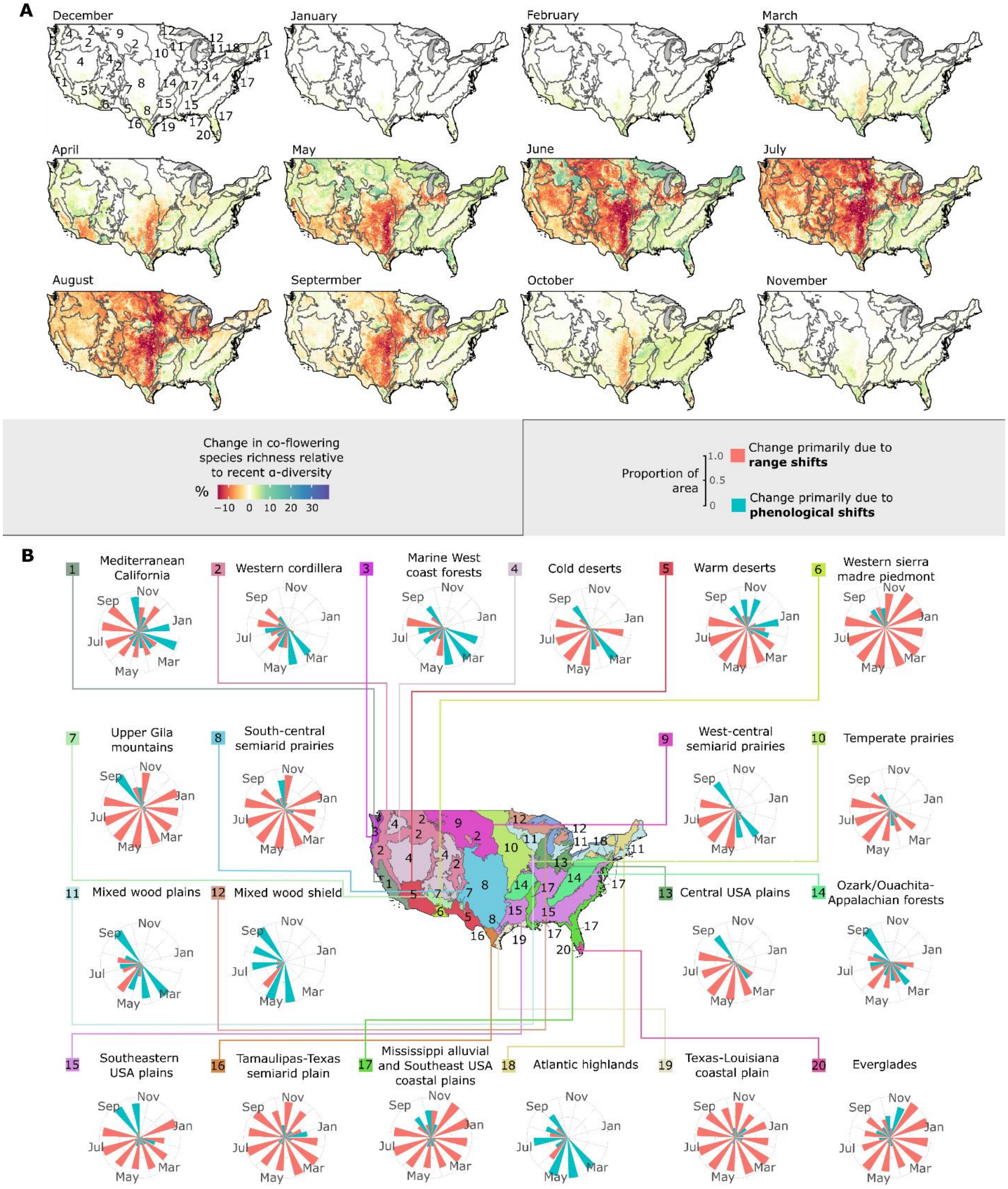

Figure 4— A Changes between recent and future environmental conditions in the richness of species flowering each month across the conterminous United States. The color scale in each panel shows the projected change in co-flowering species richness each month in each location relative to the total species richness of that site estimated under recent environmental conditions (2001-2020). Projected conditions correspond to those expected under 2 °C of warming and land cover patterns for the year 2080 under the

Special Report on Emissions Scenario (SRES) B1. **B** shows the proportion of sites within each ecoregion (map subdivisions labeled 1-20) for which range shifts or phenological shifts were the primary cause of observed changes in the diversity of flowering species that month. For graphing, the color scale was capped to the central 99% of the data to avoid distortion of the range from extreme values. Subdivisions in each panel—labeled 1-20—represent level II ecoregions. Grid cells in **A** have a resolution of 12×12 km.

Changes in patterns of pairwise flowering synchronies

Across periods, changes in the composition of pairwise flowering synchrony among species (i.e., the Bray-Curtis dissimilarity of flowering synchronies between periods) largely corresponded with those in co-flowering species richness during the peak of the season, with the greatest changes concentrated in ecoregions within central CONUS (Fig. 5A). Flowering dissimilarity between periods was more severe under projected environmental conditions than observed in recent decades, with the greatest dissimilarity observed across central CONUS, widespread but comparatively lesser shifts across Western ecoregions (especially Cold Deserts and Western Cordilleras), and relatively modest flowering dissimilarity throughout the East (Fig. 5B).

Flowering dissimilarity across periods was predominantly driven by range shifts among ecoregions (Fig. 5C). Indeed, in ecoregions showing the most severe flowering dissimilarity between periods, change across nearly all locations was primarily caused by range shifts (e.g., South-Central Semi-Arid Prairies).

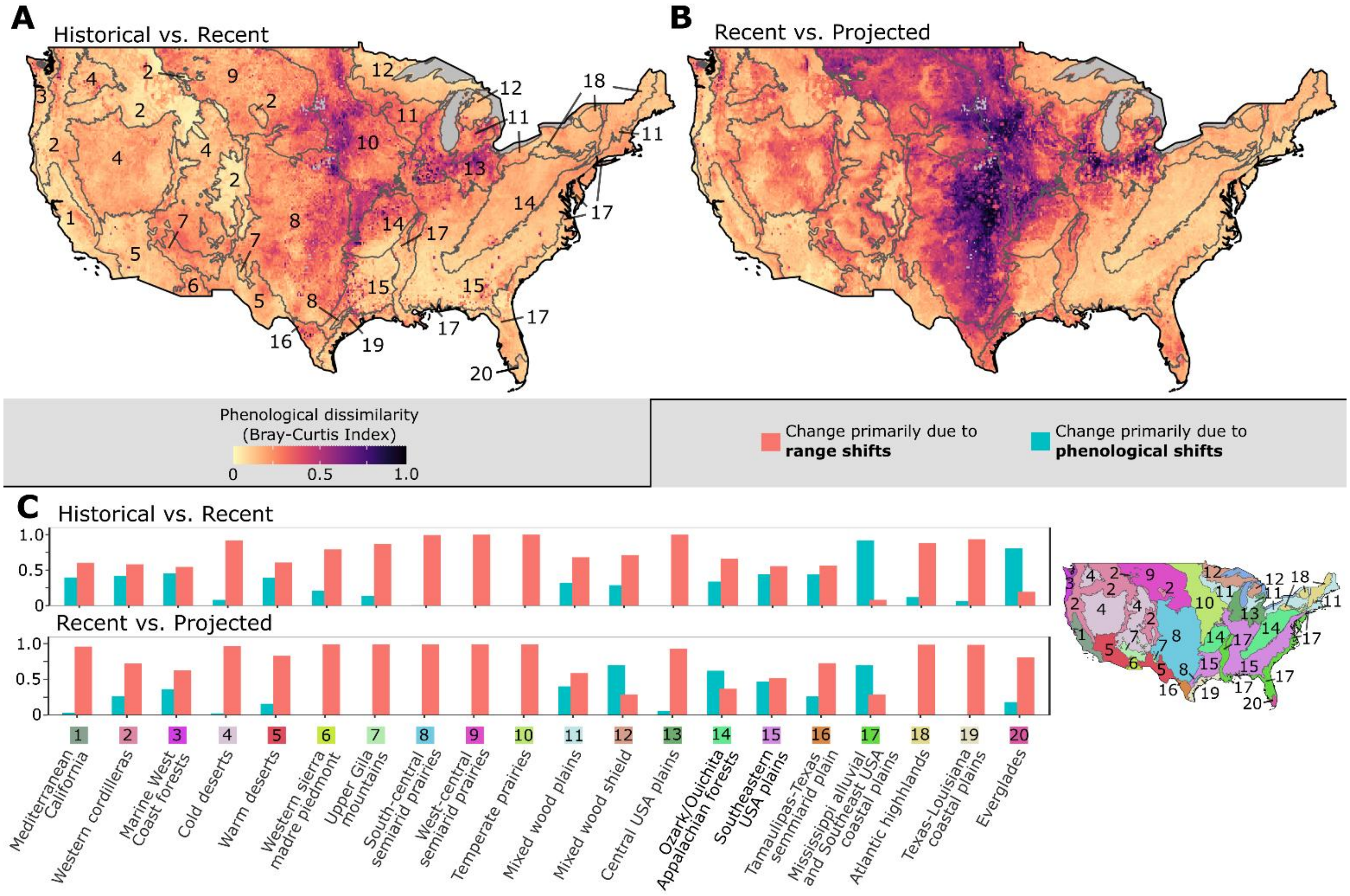

Figure 5—Dissimilarity in the composition of pairwise flowering synchronies among sympatric species. **A** shows flowering dissimilarity between the historical (1961-1980) and recent (2001-2020) periods. **B** shows flowering dissimilarity between recent and projected conditions, which correspond to those expected under 2 °C of warming and land cover patterns for the year 2080 under the Special Report on Emissions Scenario (SRES) B1. Flowering dissimilarity was measured using the Bray-Curtis Dissimilarity index, with values of 0 indicating no changes in species composition and degree of flowering overlap, and values of 1 indicating all pairs of overlapping species were gained or lost relative to the preceding period. For graphing, the color scale was capped to the central 99% of the data to avoid distortion of the range from extreme values. Subdivisions in each panel—labeled 1-20—represent level II ecoregions. **C** shows the proportion of area within each ecoregion in which either shifts in phenology or species ranges was the primary cause of flowering dissimilarity between periods.

Environmental correlates of changes to the flowering season

Historical changes in the start, end, and duration of the season were primarily associated with changes in mean annual temperature (Fig. 6A-D), with warming leading to an earlier SOS and later EOS, and therefore a longer DOS (Fig. 6A,B). These effects were more pronounced along a temperature seasonality gradient, with warming associated with greater advances in SOS in locations with higher temperature seasonality, concurrently leading to greater increases in DOS (Fig. 6D). Changes in cumulative annual precipitation were primarily associated with shifts in SOS (Fig. 6A), with variable effects along the temperature seasonality gradient (higher precipitation associated to SOS delays in seasonal locations, and with advances in aseasonal locations; Fig. 6D) and no discernible variation along the aridity gradient (Fig. 6C). However, for changes between recent and projected environmental conditions, the patterns differed: temperature was more weakly associated with shifts in SOS and DOS (Fig. 6A), and associations between phenology and warming varied along the aridity gradient, with lesser effects in arid locations (Fig. 6C).

In turn, pairwise flowering dissimilarity between periods was most strongly associated with changes in precipitation (Fig. 6E-H). For historical changes, increases in precipitation were associated with greater flowering dissimilarity, with no apparent interactions with long-term aridity or temperature seasonality across locations. Such patterns differed for changes between recent and projected conditions. Future warming and increases in crop cover were also associated with higher flowering dissimilarity (Fig. 6E,F), with temperature showing slightly stronger associations in arid locations (Fig. 6G) and in areas with low temperature seasonality (Fig. 6H). Moreover, in contrast to historical changes, decreases in precipitation were associated with greater flowering dissimilarity between periods (Fig. 6F), a pattern that was more pronounced in arid locations (Fig. 6G).

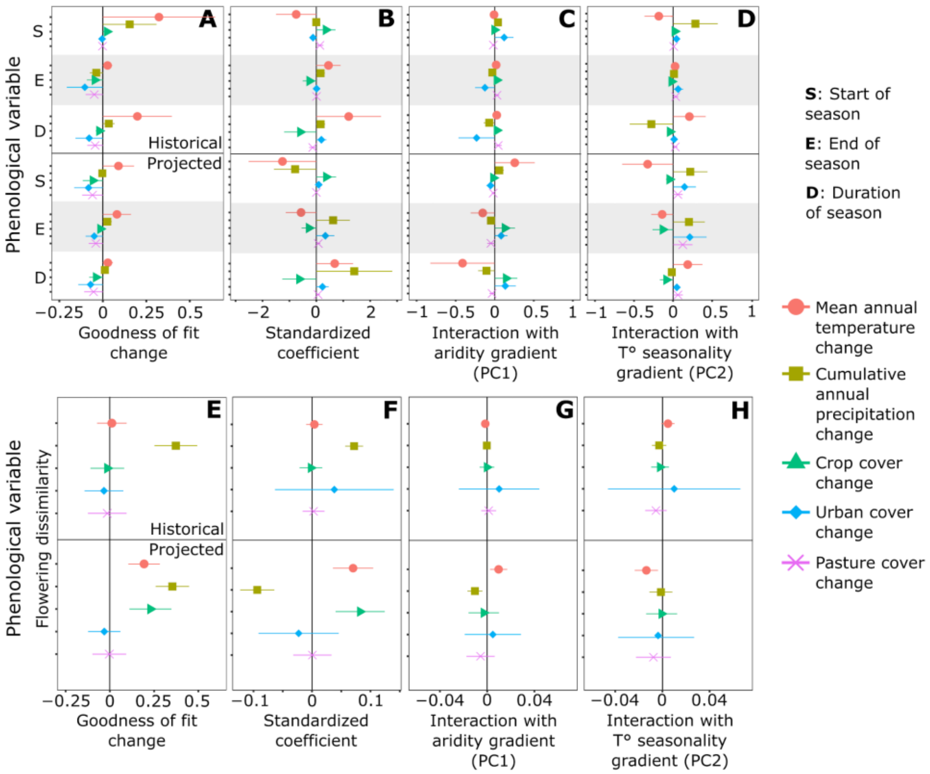

Figure 6—Flowering season versus environmental changes across sites. **A-D** show the degree to which different forms of environmental change are associated with shifts in the start, end, and duration of the season between periods, the coefficients of each type of environmental variable, and their interactions with long-term climatic conditions across sites characterized by a geographic aridity gradient (PC1) and a temperature seasonality gradient (PC2). **E-H** show the same for changes in patterns of pairwise flowering synchrony among co-occurring species. Each panel shows the distribution of each metric obtained by fitting 2,000 models using random samples of 100 locations accounting for spatial dependence among observations (points correspond to means and bars to standard deviations of each metric across iterations). Goodness of fit changes for each environmental variable were calculated from changes in the correlation of fitted versus observed values (in a test dataset) after including it in the model relative to base models accounting only for differences in long-term climatic conditions among sites (i.e., no environmental change). All environmental change variables were standardized to a standard distribution of 1 prior to fitting the models. Projected conditions correspond to those expected under 2 °C of warming and land cover patterns for the year 2080 under the Special Report on Emissions Scenario (SRES) B1.

Discussion

By analyzing millions of observations across thousands of plant species, we demonstrate that—across biomes—joint shifts in phenology and species ranges in recent decades have significantly advanced and extended the flowering season across North America. Our analyses reveal substantial seasonal redistribution of flowering diversity within communities, with co-flowering species richness typically increasing early and late in the season and decreasing during historical peaks—trends predicted to intensify under projected environmental conditions. Despite acting concurrently, shifts in phenology versus species-ranges primarily impacted different attributes of the season. Species-level phenological shifts—and temperature—were the primary drivers of changes in community-level attributes related to the timing of the flowering season, such as its start, end, and duration. In contrast, changes in species' ranges—and precipitation—were the main drivers of community-level shifts in co-flowering richness during late spring and summer and of attributes tied to community composition, such as patterns of flowering synchrony among co-occurring species. These findings outline heterogeneous macroecological impacts and mechanisms of change across North American biomes, revealing a wider suite of impacts than predicted from analysis of each process in isolation.

Shifts in phenology and species distribution jointly but distinctly impact the flowering season

As hypothesized (Fig. 1), shifts in phenology—primarily mediated by temperature—and range shifts—primarily driven by precipitation and to a lesser extent land use changes—had their greatest effects on different attributes of the flowering season at the community level. Therefore, future changes to the structure of the season across communities will depend on the relative severity of concordant shifts in phenology versus species ranges. Specifically, predominance of phenological shifts would primarily alter the timing of the flowering season and the seasonal distribution and diversity of co-flowering species, particularly at the start and end of the season. In turn, predominant effects of range shifts would alter seasonal peaks in flowering diversity and the network of flowering overlaps among species, thereby altering the potential for flowering-mediated species interactions.

The predominance of either process will likely depend on the severity of environmental trends. Limits to phenological plasticity can prevent plants from shifting development further in response to climatic trends (21). For example, studies on woody species in the temperate zone have found that phenology shifts linearly with temperature up to a warming threshold of approximately 4 °C, after which responses stall (15, 22, 23). Therefore, while average global temperature changes of 2 °C—as those considered here—might not cause widespread exhaustion of plant phenological plasticity, these constraints might be important under more extreme warming scenarios, limiting further contributions of shifts in phenology to changes in the flowering season. In contrast, shifts in demography and species ranges are likely to accelerate under more extreme environmental change (24, 25). Therefore—to the extent that the limits of phenological plasticity are similar across biomes, functional groups, and taxa—more severe climate change could cause range shifts to predominate over shifts in phenology as drivers of community-level changes, thus primarily impacting patterns of flowering synchrony and the diversity of co-flowering species during late spring and summer across communities.

Our results also reveal discrepancies between historical and projected patterns of change, including the direction and severity of changes across regions (e.g., end of season shifts in the western continental U.S.; Fig. 2), and the associations between changes in environmental conditions and community-level phenology (e.g., the relationship between precipitation change and flowering dissimilarity; Fig. 6F). For many regions, the direction of historical and projected climate change differed (Fig. S2), but such mismatches cannot explain all observed discrepancies. For example, historical and projected changes to EOS were in opposite directions among many Western ecoregions despite consistent changes in climate across periods (Fig. 2; Fig. S2), whereas EOS changes were consistent across the East despite opposing climatic trends (e.g., Fig. 5; Fig. S2). Historical and projected environmental changes occurred over different climatic and land use baselines, so such mismatches may be due to non-linear or interactive effects of environmental changes on phenology and species ranges. While we cannot identify their ultimate causes, these discrepancies show that past patterns of change may be weak predictors of future trends.

Flowering reassembly and its impacts differ across biomes

Our study corroborates previous research showing widespread advancement and lengthening of the flowering season across floras (26–28). However, we also found wide regional variation in the direction and severity of changes in the structure of the flowering season, which may cause profound ecological impacts. For example, in recent decades, the richness of co-flowering species sharply increased early and decreased later in the season in many ecoregions (e.g., Western Cordillera, Cold Deserts, Mediterranean California; Fig. 3), which could result in opposing effects on density-dependent processes such as pollinator attraction or insect foraging success during spring and summer (29, 30). In turn, some communities experienced consistent declines in flowering diversity throughout the year (e.g., areas of the South-Central Semi-Arid Prairies), which could decrease the diversity of organisms reliant on flowers across the season (31, 32). Other regions experienced consistent increases in flowering diversity throughout the year (e.g., Southeastern ecoregions), which may not affect different seasons disproportionately but could alter ecological processes through novel species interactions (6). Regardless of specific patterns, these shifts have likely altered (and may continue to alter) the selective environments encountered by plants and interacting organisms across CONUS (2).

Communities across the Great Plains appear particularly vulnerable to climate-driven restructuring of the flowering season. This region has experienced increasing aridity to the West and increasing humidity to the East of the 100th meridian West—a bioclimatic boundary dividing the humid East and arid West (33). Aridification has been linked to biomass loss, rapid species declines, and species turnover in grasslands (19, 34, 35). Climate change is predicted to exacerbate aridification trends, and conversion of grasslands to agriculture is projected to accelerate under the land use scenario considered in this study (Figs. S2,4), threatening pollinator diversity and their ecosystem services (36). In contrast, many regions–such as the Sierra Nevada, Cascades, and most Southeastern ecoregions–exhibit lower flowering reassembly despite facing aridification or substantial land cover changes (Figs. S2,4). While we cannot identify the ultimate causes of these trends, the severe impacts expected across the Great Plains might be caused by potential limits to species ranges imposed by the arid-humid bioclimatic boundary, with aridification trends leading to local extirpation of humidity-adapted species at the boundaries of their ranges (37–40).

Limitations and future directions

This study provides a unique macroecological assessment of changes to the flowering season due to the combined effects of shifts in flowering time and species ranges across North America. However, the precise ecological consequences of these effects are difficult to predict. First, we modeled shifts in the timing and diversity of flowering across scales, but not in the overall abundance of floral resources due to potential changes in species' abundances or flower production, which could amplify or reduce the ecological impacts of altered flowering times.

Relatedly, presence-background SDMs model shifts in habitat suitability without accounting for temporal lags in colonization or local extinction, or the persistence of populations in suboptimal habitat—potentially overestimating species turnover at short time scales—and do not consider changes in population sizes. Moreover, many plant communities are dominated by a few species whose flowering responses may deviate from the wider community, and ecological outcomes often depend on a handful of species interactions (e.g., specialized plant-pollinators systems) whose responses might not match those of the wider community.

Given these and other complexities, assessing the effects of climate change on floral resource production—both through individual-level crop sizes and population-level demography—is crucial to determine whether the spatiotemporal redistribution of co-flowering diversity will lead to concordant changes in floral resource availability. In turn, forecasting more precise ecological outcomes will require focusing analyses on key species based on local abundance, floral output, functional traits, or other attributes relevant to the specific ecological phenomena under study.

Despite these challenges, this study provides a promising approach for examining changes to the seasonal structure of terrestrial communities at broad spatial scales. Field datasets tracking the seasonal abundance of flowers are rare, and remote sensing methods cannot detect weak spectral signals from these structures nor identify individual species. By combining species distribution and phenological modeling and using diverse publicly available datasets, we outline a framework for estimating changes to the seasonal structure of plant communities at broad spatial scales that maintains resolution at the level of species, features that may provide valuable resources for natural resource management and conservation planning.

Materials and Methods

Phenology and occurrence data

To model flowering phenology, we compiled specimen records from 220 herbaria, accessed digitally through 16 consortia from Mexico, the U.S., and Canada (in July and August 2022) (41). Only specimens explicitly recorded as bearing flowers were retained, which we identified through the detection of unique entries in the DarwinCore ‘reproductiveCondition’ column that clearly indicated the presence of flowers. Specimens missing geographic coordinates, collection dates, or species-level identification were excluded. To avoid pseudoreplication, conspecific specimens collected within 1 km of each other on the same day were removed. Since over 92% of the remaining specimens were collected within the United States, and to match the spatial extent of land use/land cover (LULC) data used in species distribution models (SDMs), we excluded specimens collected outside CONUS. Specimens collected before 1958 were also removed to align with the temporal range of TerraClimate climate data used in the analysis. After harmonizing species names using the Global Biodiversity Information Facility (GBIF) taxonomic backbone, the data were filtered further to include only species represented by at least 100 specimens. The day of year (DOY) of collection was used as a proxy for flowering date, with an azimuthal correction applied to address the discontinuity between 31 December and 1 January, converting prior year DOYs into negative values.

To model species ranges, we obtained an additional 13.2 million research-grade occurrence records from the Global Biodiversity Information Facility (GBIF) for species well-represented in the flowering phenology dataset (accessed July 11, 2024; https://www.gbif.org/occurrence/download/0021084-240626123714530). These records, primarily from iNaturalist and herbarium sources, were combined with those from Park et al. (41). We removed duplicates using the ‘occurrenceID’ column in DarwinCore. To match the temporal and spatial extent of LULC data included in SDMs, we retained only occurrences derived from iNaturalist and herbarium records collected between 1999 and 2023, and limited the dataset to occurrences within CONUS. Preliminary analyses of GBIF occurrences revealed significant spatial biases towards urban areas and major roads. To address this, we identified occurrences within urban areas as defined by the US Census Bureau (2012) using the ‘tigris’ package v2.1 (42) . We thinned the data using the ‘spThin’ package v0.2.0 (43), keeping only occurrences of the same species recorded at least 20 km apart within urban areas. Additionally, we removed occurrences within 2 km of ‘primary roads’ mapped by the US Census Bureau in 2012. To further reduce spatial bias, another thinning step was applied, keeping only conspecifics recorded at least 5 km apart regardless of urban or road proximity. After cleaning using BONAP records (see next subsection), we retained only species with at least 50 occurrences to ensure adequate sample sizes for species distribution modeling (see ‘*Training SDMs’* section for information on how pseudo-absences were generated).

Final cleaning of specimens and occurrences using BONAP

Species misidentifications or geolocation errors in herbarium and occurrence databases can bias SDMs or phenoclimatic models by distorting the climate space or flowering dates represented among observations. To mitigate this, we removed implausible records using expertly curated data from the Biota of North America Program's (BONAP) North American Plant Atlas (NAPA) (44), which documents 19,039 taxa from 227 families across 3,067 counties across CONUS. BONAP compiles species presence/absence data from herbarium records, museums, and bibliographic reviews, most of which are verified by taxonomic and floristic experts. Species names were harmonized across the specimen, occurrence, and BONAP datasets using BONAP’s taxonomic backbone. We then excluded observations from counties where BONAP did not report occurrences for the species.

After cleaning, the final specimen-based phenology dataset included 1,042,939 specimens (collected from 1958 to 2022) representing 2,837 species in 1,042 genera and 139 families. The final occurrence dataset contained 1,673,454 records (collected from 1999 to 2023), comprising the same species, genera, and families. Of these, 1,369,657 were community science observations from iNaturalist, and 303,797 were herbarium specimens not included in ref. (41).

Climate data

We obtained historical monthly climatic rasters from TerraClimate (45) available from January 1958 to December of 2023 at a 4 × 4 km resolution. These data consisted of monthly time series for minimum temperature (TMIN), mean temperature (TMEAN), maximum temperature (TMAX), and cumulative precipitation (PPT), as well as modeled water balance metrics including actual evapotranspiration (AET), climate water deficit (DEF, potential evapotranspiration - AET), soil moisture (SOIL), and snow water equivalent (SWE).

Climate variables for species distribution modelling

We used monthly climate data to calculate annual bioclimatic variables known to influence plant distributions. For each year and location across CONUS, we computed annual means (or sums for precipitation), minimum and maximum monthly values (e.g., mean minimum temperature of the coldest month, mean maximum of the warmest month), annual ranges (difference between maximum and minimum mean monthly values), and seasonality (standard deviation of monthly values within year). For temperature, we also calculated the approximate mean diurnal temperature range (mean difference between TMAX and TMIN across months) and approximate isothermality (mean approximate diurnal range divided by the annual range). For precipitation, seasonality was calculated relative to cumulative annual precipitation within each site. Minimum monthly SWE was removed from the analyses, as it was 0 across CONUS. This resulted in 31 climate variables: 7 for temperature, 5 related to PPT, AET, DEF, SOIL, and 4 for SWE, calculated annually across all CONUS locations. For the location of each occurrence record, we computed long-term averages of these variables over the 20 years preceding its collection date. We used 20-year instead of a standard 30-year period to reduce the proximity between historical and recent conditions in our analyses of species ranges (see next sections). Additionally, we obtained elevation data from USGS at a 100m × 100m resolution, and calculated mean elevation and elevational heterogeneity within 800m × 800m grid cells. The coarser resolution for elevation was used to account for uncertainties in georeferencing of herbarium specimens, which may be problematic in steep mountainous regions where topography changes over short distances (46).

Since many of the climate variables were highly collinear (Fig. S1) and are causally related, we performed a principal component analysis (PCA) to reduce the dimensionality of the climate space. The PCA used 20-year averages of all variables for the most recent period available (2004-2023) across all 4km × 4km grid cells in CONUS. We retained the five principal components (PCs) with eigenvalues ≥ 1, which collectively explained 88.2% of the variance in the climate data (Table S1). PC1 represented a gradient of increasing aridity, PC2 a gradient of decreasing temperature and increasing temperature seasonality, and PC3 a gradient of increasing elevational heterogeneity and mean elevation with decreasing temperature seasonality. PC4 primarily captured increasing soil moisture, while PC5 reflected increasing actual evapotranspiration and elevation (Fig. S2). We then projected the 20-year average climate conditions associated with each occurrence record onto these PCA axes, reducing the number of climatic predictors from 31 variables to 5.

To predict species distributions across different periods, for each occurrence record we calculated 20-year averages for each of the 31 climate variables for a historical period (1961-1980) and a recent period (2001-2020). We also obtained projected climate conditions from TerraClimate for a scenario where global temperatures rise by 2°C above pre-industrial levels. This scenario is not tied to a specific time frame or emissions pathway; instead, TerraClimate interpolates climate normals from 1985-2015, adjusting for the changes in means and seasonality expected under 2°C of warming. We then projected historical, recent, and future climatic conditions onto the 5 principal components derived from the 2001-2020 data.

Climate variables for phenoclimatic modelling

Variation in TMEAN and PPT among sites and years of specimen collection was partitioned into spatial and temporal components by calculating long-term means (reflecting geographic differences in chronic climatic conditions) and year-specific deviations from these long-term means (reflecting interannual differences). For each species at each site and year, we obtained data for the climatic conditions during the 3-month periods leading up to its average flowering onset, peak, and termination. To estimate conditions approximately before flowering onset, we used the 10th percentile collection date across all specimens from each species and calculated the mean TMEAN and cumulative PPT for the 3 months leading up to that month. The same approach was applied for the 50th percentile (flowering median) and 90th percentile (flowering termination) collection dates. For each specimen, we characterized its site’s long-term TMEAN and PPT (normals) by averaging the observed conditions across all years between 1961 and 1990 for each 3-month period approximating that species’ flowering onset, median, and termination. We then calculated climatic deviations (anomalies) from the 1961-1990 normals in the year of each specimen's collection for these 3-month periods.

Assuming phenological changes are driven by interannual variation in TMEAN and PPT rather than by spatial phenology-climate relationships, we calculated deviations from 1961-1990 normals for all 3-month windows. This was done for the historical period (1961-1980), the recent period (2001-2020), and the future 2°C warming scenario. These TMEAN and PPT deviations were then used to predict changes in flowering onset and termination between reference periods at each species' occurrence site.

Land use and land cover data

We obtained land use and land cover (LULC) data from the National Land Cover Database (NLCD) (47), available for 2001, 2004, 2006, 2008, 2011, 2013, 2016, 2019, and 2021. The NLCD uses Landsat spectral data to classify 30m resolution grid cells into land cover and land use classes, providing a consistent, high-resolution dataset across CONUS. We separated each year's multiclass raster into layers representing the presence or absence of each LULC type. We retained all cover classes except those not recent in CONUS (e.g., lichen, moss, sedge classes from Alaska) or those that were rare (e.g., barren land). For land cover, we kept forest classes (deciduous, evergreen, mixed), scrubland (shrub/scrub), herbaceous grasslands, and wetlands (herbaceous and woody). For land use, we included four urban categories (open, low, mid, high) and two agricultural classes (cultivated crops, pasture/hay). To match the format of the LULC data available for forecasting and backcasting (see next paragraph), we aggregated all urban classes into a single category. To account for uncertainty in occurrence coordinates and because plant occurrence can be influenced by landscape context at broader scales than 30m (Mazerolle and Villard, 1999), we measured the proportion of each class cover within 750m × 750m grid cells (625 30m × 30m cells) around each occurrence. LULC class proportions were sourced from the NLCD layer closest to the year of collection for each record. These class proportions were then used as predictors in SDMs.

Because NLCD data were available only from 2001 to 2021, we obtained historical (1961-1980) and future (2061-2080) LULC projections from the Earth Resources Observation and Science Center (EROS) at a 250m resolution (48, 49). EROS' projections use the same modeling framework as NLCD, integrating land use trends with spatially explicit allocation based on regional suitability for each LULC class. Though EROS projections were based on the Special Reports Emissions Scenarios (SRES) from the IPCC (2000)—replaced later by Representative Concentration Pathways (RCP; IPCC 2013) and Shared Socioeconomic Pathways (SSP; IPCC 2021)—they align closely with RCP and SSP scenarios (50, 51). We chose the B1 scenario for forecasting, as it is the closest match to RCP4.5 and SSP2-3, representing 'middle-of-the-road' emissions and development scenarios. As with NLCD data, we calculated the proportion of each land cover class in 750m resolution blocks (containing 9 grid cells) to generate historical and future predictions used in SDMs.

Analyses

Training SDMs

Species distributions were modeled using presence-background random forest classifier models implemented in the ‘randomForest’ package v4.7-1.1 (52). Random forests are a supervised machine learning technique that uses an ensemble of decision trees to identify relationships between a response (here, presence/background data) and predictors (here, climatic and LULC variables). By combining multiple decision trees, the ensemble performs better than any single model, leveraging the "wisdom of the crowds." This approach does not require predefined model structures (e.g., linear relationships) and its non-parametric nature allows for discovering complex relationships and interactions (53). This flexibility was crucial for these analyses of thousands of species with diverse distributional responses to climate and LULC. Additionally, random forests are computationally efficient and have been demonstrated to be among the most accurate SDM methods available (54).

SDMs for each species were trained using occurrence data from 1999-2021. This period ensured availability of high-quality LULC data from NLCD within two years of each collection date. All models included the 5 bioclimatic PCs and the proportion of each LULC class around collection sites as predictors. To address the challenge of selecting pseudo-absences—where it is often unclear if unoccupied regions are due to sampling bias or true distributional patterns—we used curated BONAP records to identify counties where each species was not documented. We drew 10,000 random locations per species from these counties (excluding areas within 2km of major roads). For these locations, we obtained 20-year climatic averages (2001-2020) projected onto the 5 climatic PCs and LULC variables from a randomly selected year between 2001 and 2021. To address class imbalance, we downsampled pseudo-absences to match the number of occurrences in each initial tree. Each species-specific model used 500 trees with a maximum of 5 predictors at each split.

Decision trees are built using bootstrap samples of the data. Typically, these samples contain about 2/3 of the original data, with the remaining third (out-of-bag or 'OOB' data) used to calculate each tree's error rate (Cutler et al. 2007). We evaluated model performance by averaging the error rates across all trees, which typically provides an unbiased estimate of the model's generalization error. Specifically, we calculated the true skill statistic (TSS), which is the sum of the true positive rate (TPR) and true negative rate (TNR) minus one. The median TSS among species was 0.91 (range: 0.51 to 0.99).

The SDMs output a probability of occurrence under specific environmental conditions, derived from the proportion of trees predicting the positive class. Given that SDMs were fit with observed presences but generated pseudo-absences data, these probabilities are interpreted as habitat suitability rather than actual probabilities of occurrence. To set a suitability threshold for considering a species to be recent at a site, we calculated the receiving operating curve (ROC) for each model and determined the threshold (0-1) that maximized the true positive rate (minimizing false negatives) while keeping the false positive rate below 0.05. While this criterion maximized true positive detection at the expense of higher false negative rates, this tradeoff is justified since implausible occurrence predictions could be identified and removed using BONAP county records (see '*Species-level predictions of distributions and phenology*' subsection).

Training phenoclimatic models

For each species, we modeled how flowering onset, termination, and duration varied with long-term climatic conditions and interannual climatic variation. We used quantile regression (via the 'quantreg' package v5.97) (55) to assess how collection date distributions among conspecifics responded to geographic and interannual variations in TMEAN and PPT (i.e., normal and anomalies, respectively). We used the 10th percentile of the distribution to represent population-level flowering onset, the 90th percentile to represent flowering termination, and the interquartile distance between them to represent flowering duration. We chose the 10th and 90th percentiles and focused on well-sampled species because estimation of extreme quantiles is more strongly biased by small samples. Moreover, recent simulations show that quantile regression accurately estimates 10th and 90th percentiles of opportunistically sampled data for sample sizes similar to those in this study (56), and this approach has been effective in studying phenological distributions in both plants and insects (57, 58).

In each species-specific model, predictors included TMEAN normal, PPT normal, and their interaction for the 3-month period before the approximate date of flowering onset (10th percentile DOY among specimens) or termination (90th percentile DOY), as well as TMEAN anomaly, PPT anomaly, and their interaction during the same period (6 predictors total). The coefficients for the main terms in these quantile regressions indicate how the 10th and 90th percentiles of flowering are affected by geographic or interannual variation in TMEAN and PPT, assuming average values for interacting variables. Interaction coefficients between normals represent the degree to which long-term precipitation affects the magnitude of phenological changes due to variation in long-term TMEAN across sites (or vice versa), whereas the interaction coefficients between anomalies indicate how the effects of interannual variation in TMEAN varies among drier- or wetter-than-average years (and vice versa). This approach models phenological variation as a response to: i) geographic variation in chronic TMEAN and PPT conditions across sites, using temporally invariant normals from 1961-1990, and ii) TMEAN and PPT anomalies reflecting temporal variation within sites, which primarily capture plastic phenological responses (10). Thus, we assumed that any temporal changes in a species' flowering season within sites are driven by deviations from their 1961-1990 TMEAN and PPT normals.

Species-level predictions of distributions and phenology

Each species' SDM was used to generate habitat suitability maps for historical (1961-1980), recent (2001-2020), and future (2 °C warming, B1 LULC scenario for 2080) conditions. Climatic and LULC variables were resampled to a 12km resolution for computational ease. Suitability estimates were then converted to binary occurrence maps by applying a threshold that maximized the true positive rate (see '*Analyses—Training SDMs*' subsection). Presence-only SDMs can predict unsuitable areas outside a species' range or beyond its dispersal capacity. To address this, predictions were constrained to within 40km of counties where BONAP confirmed each species' presence, which allowed for moderate range expansion to areas adjacent to currently occupied regions between periods. These SDMs predicted substantial variation in species richness across CONUS, from 56 to 1,445 species (from a total 2,837) for the historical period (Fig. S3). Species richness was generally lowest in arid regions of the Great Plains and higher in the West compared to the East, consistent with more comprehensive assessments of plant diversity in North America (59).

Each species’ phenoclimatic model was used to predict flowering onset, termination, and duration for each location where the species was projected to occur during historical, recent, and future periods. This was done by applying deviations of average TMEAN and PPT conditions from the 1961-1990 normals for each period. Climate rasters were resampled to a 12km resolution before estimating phenological onset, termination, and duration for each site and period.

Changes in community composition and flowering structure

The SDM and phenoclimatic modeling provided predictions for species presence, flowering onset, and termination under historical, recent, and future conditions. We used these predictions to measure changes in species composition. Next, we examined changes in the start, end, and duration of the flowering season across these periods. The onset of the flowering season was defined as the DOY when 5% of species had started flowering (5th percentile), and the end as the DOY when 95% of species had ceased flowering, with duration as the span between these dates. For each location, we calculated the difference in days for the season's start, end, and duration between historical and recent conditions, and between recent and future conditions. We also measured changes in the richness of flowering species each month by calculating the proportional difference in species numbers under historical versus recent and recent versus future conditions, relative to local species richness in the preceding period.

Finally, we assessed how patterns of flowering synchrony among species change in response to environmental trends. For each location, we first calculated the overlap in flowering periods between each pair of species in each period, calculating changes in overlap between historical and recent conditions, or recent and future conditions. Flowering overlap ranged from 0 (no overlap) to 1 (identical and fully overlapping flowering dates). For species recent in one period but not the other, all flowering synchronies were set to 0 for the period in which it was absent. Using these pairwise overlaps, we measured changes in flowering synchrony within each community using the Bray-Curtis Dissimilarity Index (BCI) (60). While BCI is typically used to assess species composition dissimilarity between communities using abundance data, it is also applicable to other categorical data. In this context, BCI measured compositional differences in flowering overlaps between periods, with species pairs analogous to species and their degree of flowering synchrony analogous to abundance. Therefore, the BCI provides an integrated measure of changes in both the identity and degree of overlap among species pairs, with values ranging from 0 (complete similarity) to 1 (complete dissimilarity) between periods for each community.

Phenology versus range shifts as drivers of community-level phenological change

To assess the relative contributions of shifts in phenology and species ranges to the resulting shifts in structure of the flowering season in each location, we generated predictions of community level change assuming that either i) phenology changed but species distributions remained constant between periods, or ii) phenology remained constant but distributions changed between periods. For example, for scenarios in which only phenology shifted between historical and recent periods (i.e., 1961-1980 to 2001-2020), we generated species ranges predicted using historical climate and LULC conditions, and compared flowering dates predicted under historical versus recent conditions within these historical ranges. For each attribute of the season—and for all comparisons between historical, recent, and projected environmental conditions—we then calculated the difference between estimates of change generated by shifts in both species ranges and phenology (shown in the main text) and those obtained by allowing only phenology or distributions to shift. Changes in community-level attributes of the season ta location was classified as predominantly driven by phenological shifts if closest to the magnitude of change generated by allowing only phenology to change, or classified as predominantly driven by range shifts if closest to the magnitude of change generated by allowing only distributions to change. Finally, to assess the predominance of phenological versus range shifts as drivers of change across biomes, we calculated the proportion of grid cells in each Level II ecoregion within

CONUS for which each process was the predominant driver of observed changes. When doing this for changes in the richness of flowering species each month, we excluded locations showing shifts of less than 0.01 (corresponding to 1% of local species richness) as those overwhelmingly corresponded to areas where the flowering season had not yet started or had already ended.

Environmental change versus community-level phenological change

We evaluated the degree to which changes to the flowering season across CONUS are associated with changes in temperature and precipitation or in land cover types severely altered by human activities (i.e., urban, crop, and pasture cover). Specifically, we used generalized least squares to fit spatial regressions, each including as a response changes in either the start, end, or duration of the season, or the composition of pairwise of flowering synchronies among co-occurring species (both between historical and recent conditions, and between recent and projected conditions). Spatial dependence among observations was modeled using a gaussian correlation structure. However, because spatial regression requires computing a pairwise distance matrix among observations, computing time grows exponentially with sample size and became prohibitive at the continental scales of these analyses (encompassing over 50,000 locations at a 12km ×12km resolution). Therefore, we used an iterative approach in which models were fit using 100 locations sampled randomly across CONUS and their performance evaluated using another, equally-sized sample, repeating the process a total of 2,000 times (a number sufficiently large for the distribution of each metric to remain unaltered by further iterations, indicating adequate sampling of the predictor space).

In each iteration, we first fit base models that only included geographic variation in historical climatic conditions as predictors, including the position of each sampled location along PC1 (an aridity gradient) and PC2 (a temperature seasonality and decreasing temperature gradient) for the 1961-1980 period. These models therefore quantified how observed changes in community-level phenology varied among locations with different underlying climates without accounting for environmental change. Then, for each form of phenological change considered, we fit additional spatial regressions that included either changes in mean annual temperature, cumulative annual precipitation, crop cover, urban cover, or pasture cover in each location as predictors. These models also included two-way interactions between the environmental change variable included and PC1 or PC2 (i.e., with long-term climatic conditions), and a three-way interaction with both PC1 and PC2. These terms measured how associations between the focal types of community-level phenological change and of environmental change differed along long-term climatic gradients. For each of these regressions (and in each iteration), we assessed how the explanatory power of the model changed by including the focal form of environmental change as a predictor. Specifically, we assessed how the correlation between predicted and observed change in the test dataset improved after including the focal change variable relative to the base models that accounted only for long-term climatic conditions. We also retained the coefficients for the main effects and interactions terms from each model and their p-values. The overall effect of each form of environmental change was evaluated from the distribution of values for each metric across iterations (with means and standard deviations reported in the main text).

Acknowledgements

This work was supported by the National Science Foundation through NSF DEB-1556768 (S.J.M. and I.W.P.), NSF DEB-2105932 (S.J.M. and I.W.P.), NSF DEB-2105907 (S.R.) and NSF DEB-2105903 (C.C.D.). T.H.R.-P. is grateful to the University of California, Santa Barbara, for fellowship support in the year this manuscript was completed. We thank the many herbaria, including botanists, staff and volunteers, who collected, curated and digitized the vast volumes of herbarium specimens and community-science records leveraged for this study. We thank Elsa Cleland and Leander Anderegg for their insightful feedback on earlier versions of this manuscript.

Data and code availability statement

The underlying data used in the analyses—as well as all resulting estimates of species ranges and spatially explicit phenological predictions—will be made publicly available on Dryad upon publication of this study. All code underlying the analyses will be publicly accessible through Zenodo.

References

1. T. H. Roulston, K. Goodell, The Role of Resources and Risks in Regulating Wild Bee Populations. *Annu. Rev. Entomol.* **56**, 293–312 (2011).

2. J. A. Elzinga, *et al.*, Time after time: flowering phenology and biotic interactions. *Trends Ecol. Evol.* **22**, 432–439 (2007).

3. E. E. Cleland, I. Chuine, A. Menzel, H. A. Mooney, M. D. Schwartz, Shifting plant phenology in response to global change. *Trends Ecol. Evol.* **22**, 357–365 (2007).

4. A. E. Kelly, M. L. Goulden, Rapid shifts in plant distribution with recent climate change. *Proc. Natl. Acad. Sci.* **105**, 11823–11826 (2008).

5. E. J. Theobald, I. Breckheimer, J. HilleRisLambers, Climate drives phenological reassembly of a mountain wildflower meadow community. *Ecology* **98**, 2799–2812 (2017).

6. S. S. Renner, C. M. Zohner, Climate Change and Phenological Mismatch in Trophic Interactions Among Plants, Insects, and Vertebrates. *Annu. Rev. Ecol. Evol. Syst.* **49**, 165–182 (2018).

7. C. Parmesan, M. E. Hanley, Plants and climate change: complexities and surprises. *Ann. Bot.* **116**, 849–864 (2015).

8. P. J. CaraDonna, A. M. Iler, D. W. Inouye, Shifts in flowering phenology reshape a subalpine plant community. *Proc. Natl. Acad. Sci.* **111**, 4916–4921 (2014).

9. D. S. Park, *et al.*, Herbarium specimens reveal substantial and unexpected variation in phenological sensitivity across the eastern United States. *Philos. Trans. R. Soc. B Biol. Sci.* **374**, 20170394 (2019).

10. T. H. Ramirez-Parada, *et al.*, Plasticity and not adaptation is the primary source of temperature-mediated variation in flowering phenology in North America. *Nat. Ecol. Evol.* **8**, 467–476 (2024).

11. A. A. Wolf, E. S. Zavaleta, P. C. Selmants, Flowering phenology shifts in response to biodiversity loss. *Proc. Natl. Acad. Sci.* **114**, 3463–3468 (2017).

12. O. Godoy, D. M. Richardson, F. Valladares, P. Castro-Díez, Flowering phenology of invasive alien plant species compared with native species in three Mediterranean-type ecosystems. *Ann. Bot.* **103**, 485–494 (2009).

13. M. A. Zettlemoyer, E. H. Schultheis, J. A. Lau, Phenology in a warming world: differences between native and non-native plant species. *Ecol. Lett.* **22**, 1253–1263 (2019).

14. T. H. Ramirez-Parada, I. W. Park, S. Record, C. C. Davis, S. J. Mazer, Scaling flowering onset and duration responses among species predicts phenological community reassembly under warming. *Ecosphere* **16**, e70070 (2025).

15. A. K. Ettinger, Winter temperatures predominate in spring phenological responses to warming. *Nat. Clim. Change* **10** (2020).

16. T. M. Crimmins, M. A. Crimmins, C. David Bertelsen, Complex responses to climate drivers in onset of spring flowering across a semi-arid elevation gradient. *J. Ecol.* **98**, 1042–1051 (2010).

17. S. J. Mazer, K. L. Gerst, E. R. Matthews, A. Evenden, Species-specific phenological responses to winter temperature and precipitation in a water-limited ecosystem. *Ecosphere* **6**, art98 (2015).

18. H. Yang, *et al.*, Community structure and composition in response to climate change in a temperate steppe. *Glob. Change Biol.* **17**, 452–465 (2011).

19. E. E. Cleland, *et al.*, Sensitivity of grassland plant community composition to spatial vs. temporal variation in precipitation. *Ecology* **94**, 1687–1696 (2013).

20. M. N. Van Dyke, J. M. Levine, N. J. B. Kraft, Small rainfall changes drive substantial changes in plant coexistence. *Nature* **611**, 507–511 (2022).

21. T. Rutishauser, J. Luterbacher, C. Defila, D. Frank, H. Wanner, Swiss spring plant phenology 2007: Extremes, a multi-century perspective, and changes in temperature sensitivity. *Geophys. Res. Lett.* **35**, 2007GL032545 (2008).

22. Y. H. Fu, *et al.*, Declining global warming effects on the phenology of spring leaf unfolding. *Nature* **526**, 104–107 (2015).

23. J. Guo, *et al.*, Meta-analytic and experimental evidence that warmer climate leads to shift from advanced to delayed spring phenology. *Agric. For. Meteorol.* **342**, 109721 (2023).

24. B. Huntley, How Plants Respond to Climate Change: Migration Rates, Individualism and the Consequences for Plant Communities. *Ann. Bot.* **67**, 15–22 (1991).

25. K. J. Feeley, M. R. Silman, Land-use and climate change effects on population size and extinction risk of Andean plants. *Glob. Change Biol.* **16**, 3215–3222 (2010).

26. D. Li, *et al.*, Climate, urbanization, and species traits interactively drive flowering duration. *Glob. Change Biol.* **27**, 892–903 (2021).

27. Z. Zhou, *et al.*, Lengthened flowering season under climate warming: Evidence from manipulative experiments. *Agric. For. Meteorol.* **312**, 108713 (2022).

28. Y. Chen, *et al.*, Warming reduced flowering synchrony and extended community flowering season in an alpine meadow on the Tibetan Plateau. *Ecology* **104**, e3862 (2023).

29. M. Schenk, J. Krauss, A. Holzschuh, Desynchronizations in bee–plant interactions cause severe fitness losses in solitary bees. *J. Anim. Ecol.* **87**, 139–149 (2018).

30. D. Sponsler, A. Iverson, I. Steffan-Dewenter, Pollinator competition and the structure of floral resources. *Ecography* **2023**, e06651 (2023).

31. S. G. Potts, B. Vulliamy, A. Dafni, G. Ne'eman, P. Willmer, Linking bees and flowers: how do floral communities structure pollinator communities? *Ecology* **84**, 2628–2642 (2003).

32. J. Fründ, K. E. Linsenmair, N. Blüthgen, Pollinator diversity and specialization in relation to flower diversity. *Oikos* **119**, 1581–1590 (2010).

33. R. Seager, *et al.*, Whither the 100th Meridian? The Once and Future Physical and Human Geography of America's Arid–Humid Divide. Part II: The Meridian Moves East. *Earth Interact.* **22**, 1–24 (2018).

34. J. M. Chase, M. A. Leibold, A. L. Downing, J. B. Shurin, The Effects of Productivity, Herbivory, and Plant Species Turnover in Grassland Food Webs. *Ecology* **81**, 2485–2497 (2000).

35. A. S. MacDougall, *et al.*, Widening global variability in grassland biomass since the 1980s. *Nat. Ecol. Evol.* 1–12 (2024). https://doi.org/10.1038/s41559-024-02500-x.

36. B. A. Woodcock, *et al.*, Meta-analysis reveals that pollinator functional diversity and abundance enhance crop pollination and yield. *Nat. Commun.* **10**, 1481 (2019).

37. P. W. Barnes, A. T. Harrison, Species distribution and community organization in a Nebraska Sandhills mixed prairie as influenced by plant/soil-water relationships. *Oecologia* **52**, 192–201 (1982).

38. H. e. Epstein, W. k. Lauenroth, I. c. Burke, D. p. Coffin, Ecological responses of dominant grasses along two climatic gradients in the Great Plains of the United States. *J. Veg. Sci.* **7**, 777–788 (1996).

39. L. D. L. Anderegg, J. HilleRisLambers, Drought stress limits the geographic ranges of two tree species via different physiological mechanisms. *Glob. Change Biol.* **22**, 1029–1045 (2016).

40. M. Berdugo, *et al.*, Global ecosystem thresholds driven by aridity. *Science* **367**, 787–790 (2020).

41. I. Park, *et al.*, Herbarium-Derived Phenological Data in North America. Dryad. https://doi.org/10.25349/D9WP6S. Deposited 20 September 2023.

42. K. Walker, tigris: An R Package to Access and Work with Geographic Data from the US Census Bureau. *R J.* (2016).

43. M. E. Aiello-Lammens, R. A. Boria, A. Radosavljevic, B. Vilela, R. P. Anderson, spThin: an R package for spatial thinning of species occurrence records for use in ecological niche models. *Ecography* **38**, 541–545 (2015).

44. J. T. Kartesz, The Biota of North America Program (BONAP). *North Am. Plant Atlas Httpwwwbonapnettdc Chap. Hill NC Maps Gener. Kartesz JT 2015 Florist. Synth. N. Am. Version 10 Biota N. Am. Program BONAP* (2024).

45. J. T. Abatzoglou, S. Z. Dobrowski, S. A. Parks, K. C. Hegewisch, TerraClimate, a high-resolution global dataset of monthly climate and climatic water balance from 1958–2015. *Sci. Data* **5**, 170191 (2018).

46. D. E. Gamble, S. J. Mazer, Spatial uncertainty in herbarium data: simulated displacement but not error distance alters estimates of phenological sensitivity to climate in a widespread California wildflower. *Ecography* **2022**, e06107 (2022).

47. Jon Dewitz, National Land Cover Database (NLCD) 2019 Products (ver. 3.0, February 2024). U.S. Geological Survey. https://doi.org/10.5066/P9KZCM54. Deposited 29 February 2024.

48. T. L. Sohl, *et al.*, Spatially explicit modeling of 1992–2100 land cover and forest stand age for the conterminous United States. *Ecol. Appl.* **24**, 1015–1036 (2014).

49. T. Sohl, *et al.*, Modeled historical land use and land cover for the conterminous United States. *J. Land Use Sci.* **11**, 476–499 (2016).

50. J. Rogelj, M. Meinshausen, R. Knutti, Global warming under old and new scenarios using IPCC climate sensitivity range estimates. *Nat. Clim. Change* **2**, 248–253 (2012).

51. K. Riahi, *et al.*, The Shared Socioeconomic Pathways and their energy, land use, and greenhouse gas emissions implications: An overview. *Glob. Environ. Change* **42**, 153–168 (2017).

52. A. Liaw, M. Wiener, Classification and Regression by randomForest. *R News* **2** (2002).

53. D. R. Cutler, *et al.*, Random Forests for Classification in Ecology. *Ecology* **88**, 2783–2792 (2007).

54. R. Valavi, G. Guillera-Arroita, J. J. Lahoz-Monfort, J. Elith, Predictive performance of presence-only species distribution models: a benchmark study with reproducible code. *Ecol. Monogr.* **92**, e01486 (2022).

55. R. Koenker, V. Chernozhukov, X. He, L. Peng, Eds., *Handbook of Quantile Regression* (Chapman and Hall/CRC, 2017).

56. I. W. Park, *et al.*, Herbarium data accurately predict the timing and duration of population-level flowering displays. *Ecography* e06961 (2024). https://doi.org/10.1111/ecog.06961.

57. M. W. Belitz, E. A. Larsen, V. Shirey, D. Li, R. P. Guralnick, Phenological research based on natural history collections: Practical guidelines and a lepidopteran case study. *Funct. Ecol.* **37**, 234–247 (2023).

58. M. W. Austin, *et al.*, Climate change increases flowering duration, driving phenological reassembly and elevated co-flowering richness. *New Phytol.* **243**, 2486–2500 (2024).

59. B. H. Daru, Predicting undetected native vascular plant diversity at a global scale. *Proc. Natl. Acad. Sci.* **121**, e2319989121 (2024).

60. J. R. Bray, J. T. Curtis, An Ordination of the Upland Forest Communities of Southern Wisconsin. *Ecol. Monogr.* **27**, 326–349 (1957).

Supplemental Information for: Shifts in phenology and species ranges restructure the flowering season across North America

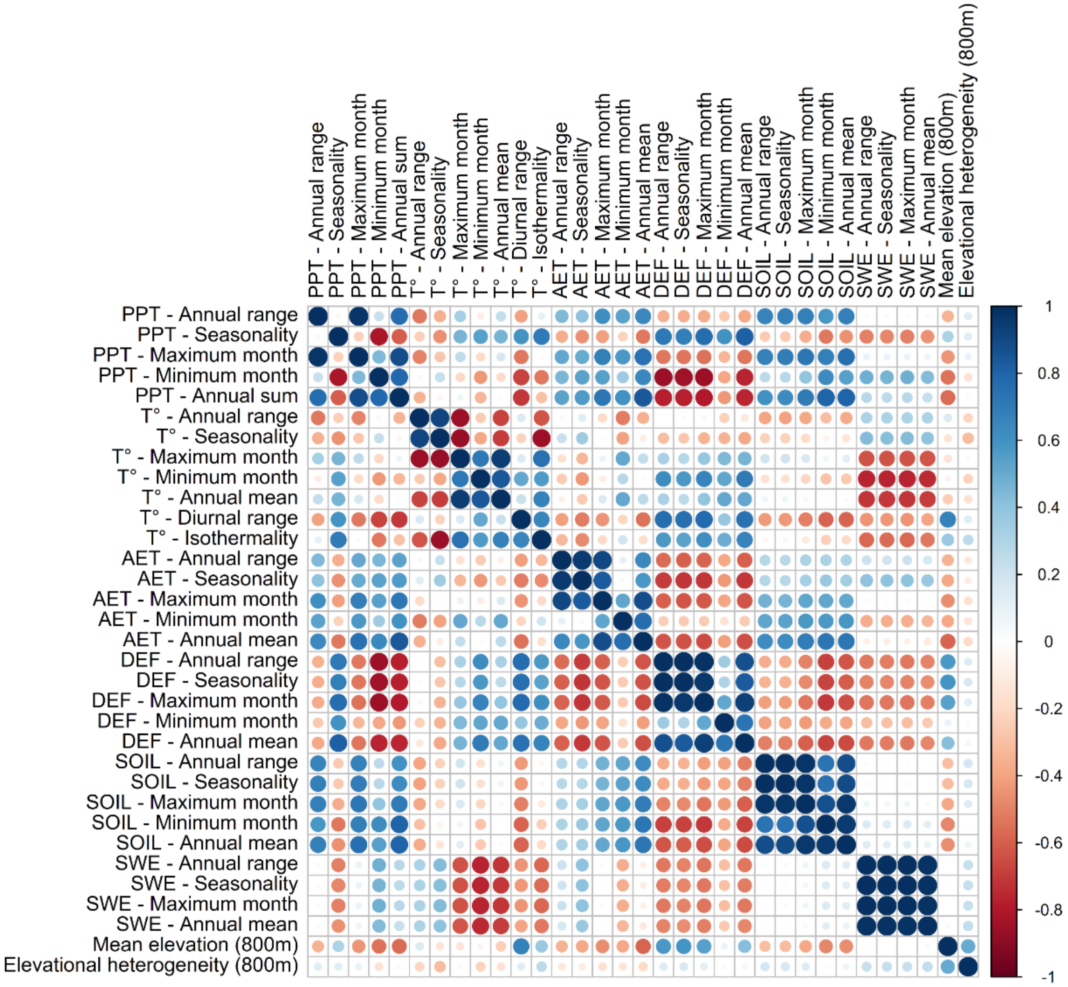

Figure S1—Correlations among 2004-2023 normals for 31 climatic variables, mean elevation, and elevation heterogeneity across 4km resolution grid cells throughout the conterminous United States. Climate variables include annual sums or means, maximum monthly values, minimum monthly values, annual monthly range, and seasonality for precipitation (PPT), temperature (T°), actual evapotransporation (AET), climate water deficit (DEF), soil moisture (SOIL), and snow-water equivalent (SWE). Variables for T° also include approximate mean daily range, and isothermality. Seasonality for precipitation was calculated proportionally to the mean cumulative annual precipitation in each site.

	PC1 (1.9, 43%)	**PC2 (1.7, 43%)**	**PC3 (1.3, 9%)**	**PC4 (1.2, 6%)**	**PC5 (1.1, 5%)**
PPT - Annual range	-0.15	-0.21	0.14	-0.05	**0.22**
PPT - Seasonality	0.20	-0.10	0.10	-0.11	0.18
PPT - Monthly maximum	-0.19	-0.18	0.10	-0.09	0.16
PPT - Monthly minimum	-0.22	0.02	-0.11	-0.17	-0.20
PPT - Annual sum	**-0.23**	-0.12	0.01	-0.10	-0.03
T° - Annual range	0.01	**0.27**	-0.20	**0.29**	0.08
T° - Seasonality	-0.07	**0.26**	**-0.25**	0.23	0.00
T° - Monthly minimum	0.08	**-0.30**	0.04	-0.22	-0.07
T° - Monthly maximum	0.16	-0.20	-0.20	-0.02	-0.03
T° - Annual mean	0.09	**-0.29**	-0.12	-0.22	-0.05
T° - Diurnal range	0.21	-0.01	0.04	0.10	0.19
T° - Isothermality	0.16	-0.21	0.18	-0.16	0.12
AET - Annual range	-0.17	-0.02	-0.19	-0.11	**0.49**
AET - Seasonality	-0.20	0.04	-0.15	-0.12	**0.42**
AET - Monthly maximum	-0.19	-0.13	-0.19	-0.07	**0.35**
AET- Monthly minimum	-0.09	**-0.26**	-0.06	0.06	-0.15
AET - Annual mean	-0.20	-0.19	-0.16	0.02	0.07
DEF - Annual range	**0.24**	-0.04	0.08	0.15	0.11
DEF - Seasonality	**0.24**	-0.03	0.10	0.19	0.09
DEF - Monthly maximum	**0.25**	-0.05	0.07	0.06	0.07
DEF- Monthly minimum	0.16	-0.06	-0.02	**-0.38**	-0.16
DEF - Annual mean	**0.25**	-0.06	0.03	-0.11	-0.02

SOIL - Annual range	-0.16	-0.18	0.21	**0.27**	0.01
SOIL - Seasonality	-0.16	-0.18	**0.21**	**0.26**	-0.01
SOIL - Monthly maximum	-0.19	-0.17	0.18	**0.23**	-0.06
SOIL - Monthly minimum	-0.21	-0.13	0.08	0.11	-0.19
SOIL - Annual mean	-0.21	-0.16	0.14	0.16	-0.15
SWE - Annual range	-0.14	0.24	0.21	-0.19	-0.02
SWE - Seasonality	-0.14	0.24	0.21	-0.20	-0.02
SWE - Monthly maximum	-0.14	0.24	0.21	-0.19	-0.02
SWE – Annual mean	-0.13	0.24	**0.22**	-0.21	-0.02
Mean Elevation (800m)	0.14	0.10	**0.28**	0.13	**0.25**
Elevational heterogeneity (800m)	0.01	0.01	**0.46**	-0.02	0.19

Table S1—Loadings from a principal component analysis (PCA) of 2004-2023 normals for 31 climatic variables, mean elevation, and elevation heterogeneity across 4km resolution grid cells throughout the conterminous United States. Loadings are reported for the 5 principal components (PCs) explaining more variance than any input variable in the data. Highlighted values in each column correspond to the 5 input variables with the highest loadings on each PC. Values next to each PC’s name in the column headings indicate its eigenvalue and variance explained.

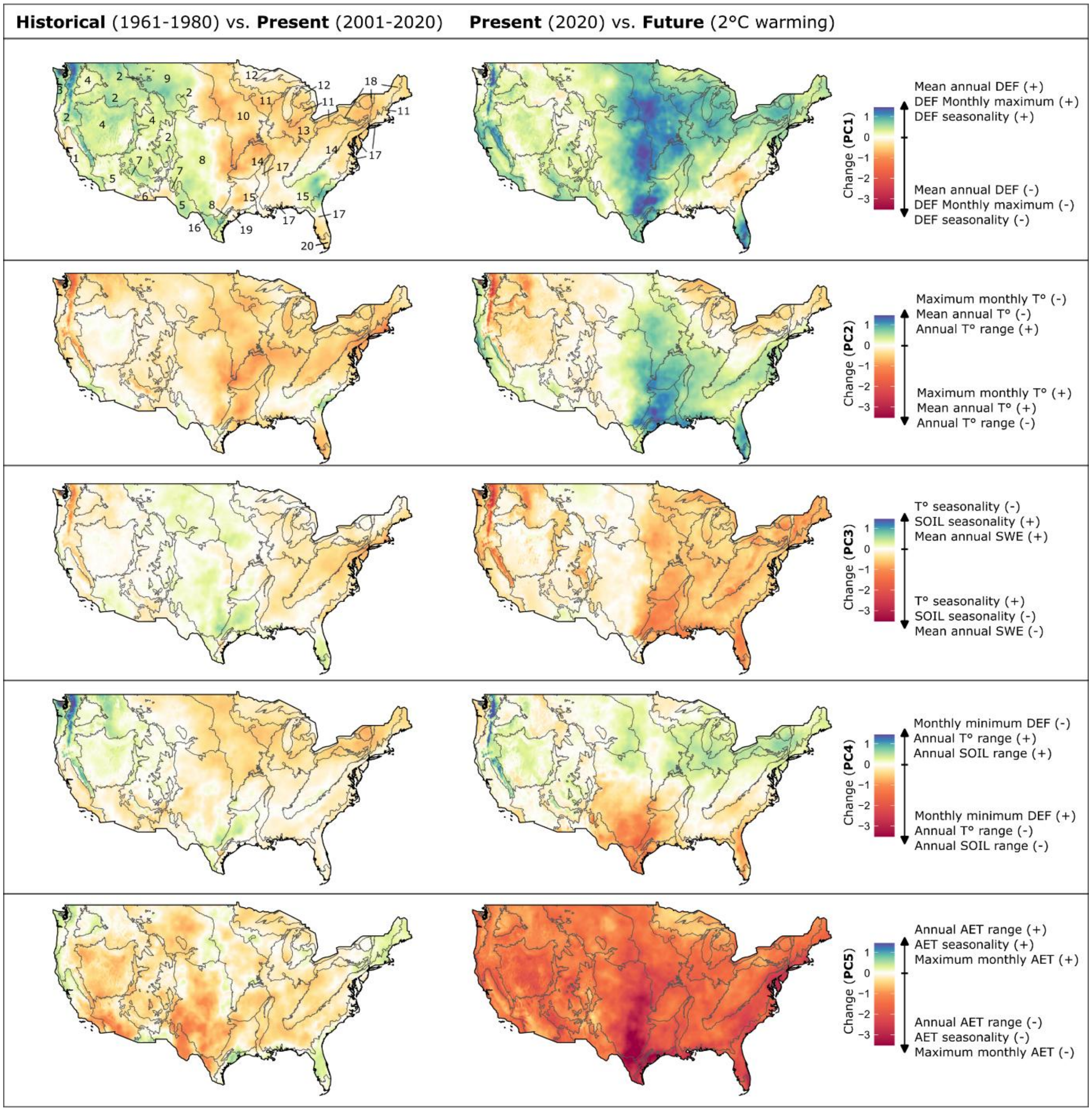

Figure S2—Climate change between the historical period (1960-1980) and the present period (2001-2020), and between the present period and projected conditions under a scenario of 2°C warming above pre-industrial levels. Climate change is shown as the difference in the 5 principal components summarizing 31 climatic variables, as well as mean elevation and elevational heterogeneity within 4km grid cells throughout the conterminous United States (see ‘*Methods*’ section of the main text) between periods. The variables listed in each legend correspond to those with the greatest loadings for each PC. Positive and negative signs next to each variable indicate whether positive or negative values in the color scale are associated to increases or decreases between periods. Subdivisions labeled 1-18 represent level II ecoregions. *1) Mediterranean California, 2) Western Cordillera, 3) Marine West Coast Forest, 4) Cold Deserts, 5) Warm Deserts, 6) Western Sierra Madre Piedmont, 7) Upper Gila Mountains, 8) South-Central Semi-*

arid Prairies, 9) West-Central Semi-arid Prairies, 10) Temperate Prairies, 11) Mixed Wood Plains, 12) Mixed Wood Shield, 13) Central USA Plains, 14) Ozark, Ouachita-Appalachian Forests, 15) Southeastern USA Plains, 16) Tamaulipas-Texas Semi-arid Plains, 17) Mississippi Alluvial and Southeast USA Coastal Plain, 18) Atlantic Highlands.

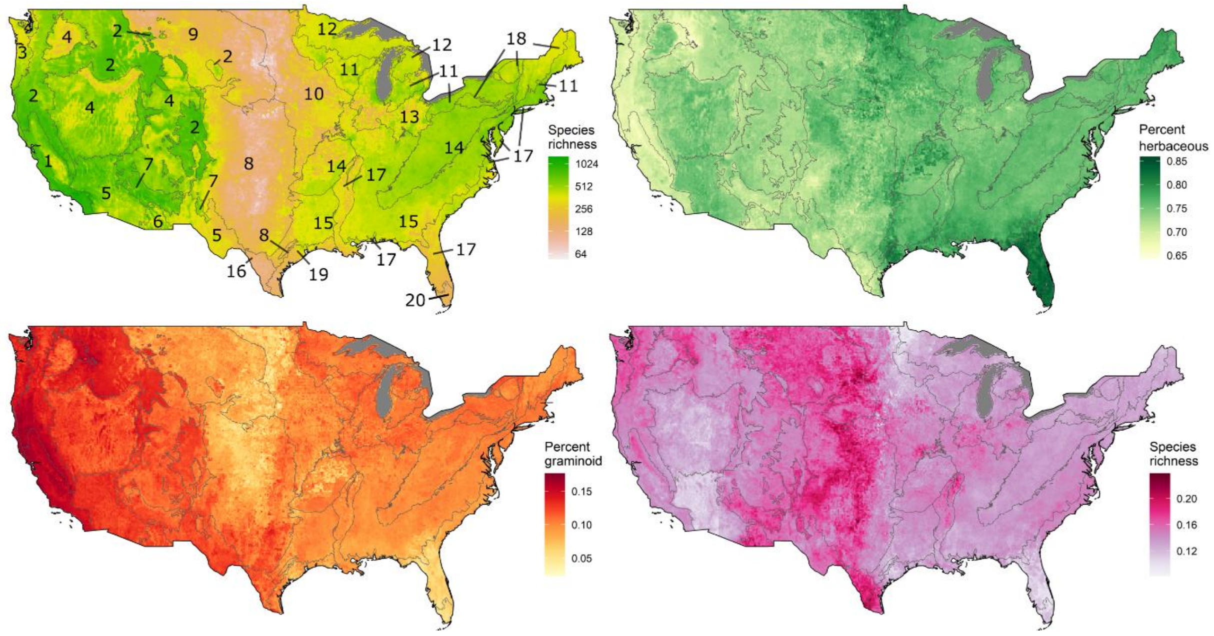

Figure S3—Predicted species richness (from a total of 2,837 species) within 12km resolution grid cells across the conterminous United States estimated for the 2001-2020 period, and the percent that have herbaceous, graminoid, or woody growth habit. Subdivisions labeled 1-18 represent level II ecoregions. *1) Mediterranean California, 2) Western Cordillera, 3) Marine West Coast Forest, 4) Cold Deserts, 5) Warm Deserts, 6) Western Sierra Madre Piedmont, 7) Upper Gila Mountains, 8) South-Central Semi-arid Prairies, 9) West-Central Semi-arid Prairies, 10) Temperate Prairies, 11) Mixed Wood Plains, 12) Mixed Wood Shield, 13) Central USA Plains, 14) Ozark, Ouachita-Appalachian Forests, 15) Southeastern USA Plains, 16) Tamaulipas-Texas Semi-arid Plains, 17) Mississippi Alluvial and Southeast USA Coastal Plain, 18) Atlantic Highlands*.

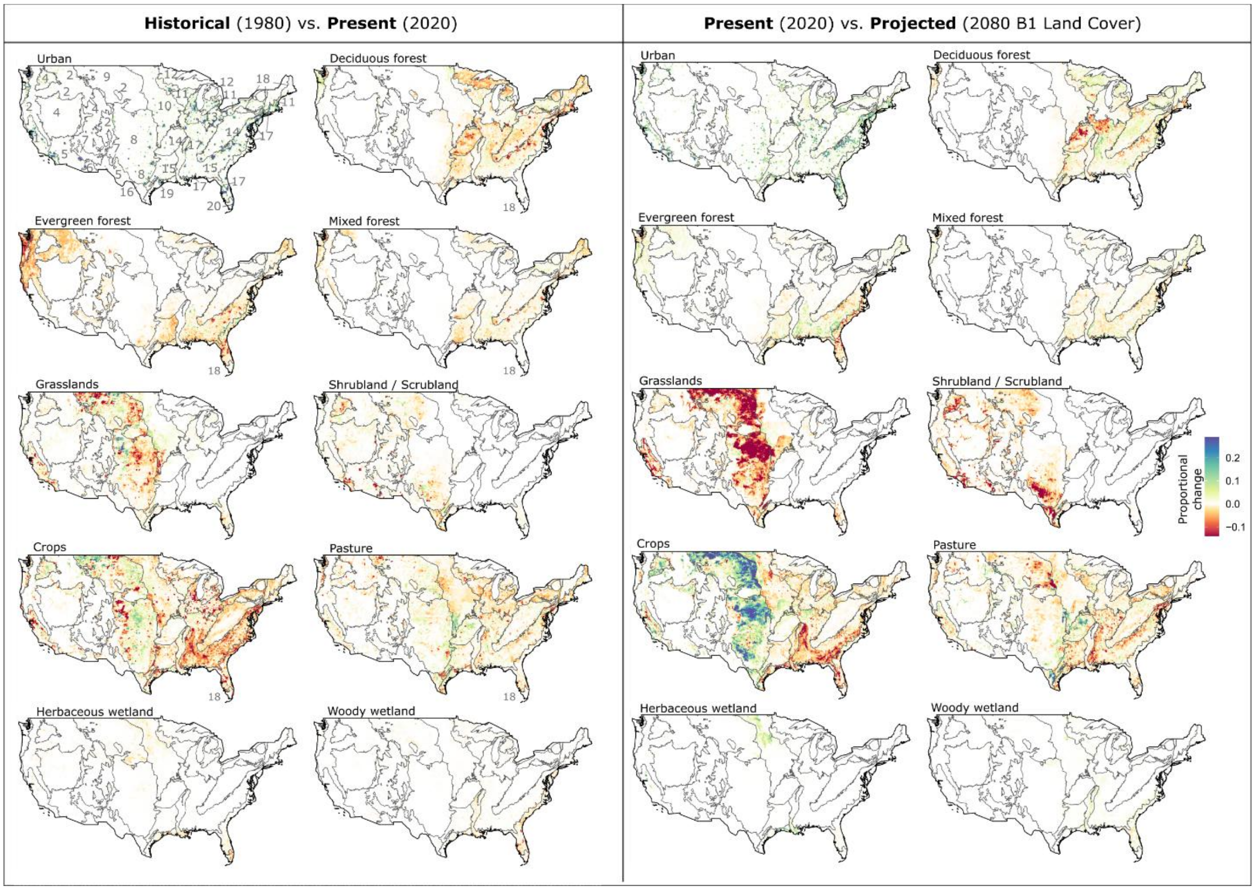

Figure S4—Change in land cover between 1980 and 2020, and between 2020 and 2080 under SRES B1 scenario of land use and land cover change. Each panel shows changes in the proportion of 250m cells of the focal class found within each 750m resolution grid cell across the conterminous United States (CONUS). Subdivisions labeled 1-18 represent level II ecoregions. *1) Mediterranean California, 2) Western Cordillera, 3) Marine West Coast Forest, 4) Cold Deserts, 5) Warm Deserts, 6) Western Sierra Madre Piedmont, 7) Upper Gila Mountains, 8) South-Central Semi-arid Prairies, 9) West-Central Semi-arid Prairies, 10) Temperate Prairies, 11) Mixed Wood Plains, 12) Mixed Wood Shield, 13) Central USA Plains, 14) Ozark, Ouachita-Appalachian Forests, 15) Southeastern USA Plains, 16) Tamaulipas-Texas Semi-arid Plains, 17) Mississippi Alluvial and Southeast USA Coastal Plain, 18) Atlantic Highlands*.